Pramana – J. Phys. (2018) 91:34
https://doi.org/10.1007/s12043-018-1611-4

Tailoring multilayer quantum wells for spin devices

S ULLAH[1,2,*], G M GUSEV[1], A K BAKAROV[3] and F G G HERNANDEZ[1]

[1]Instituto de Física, Universidade de São Paulo, Caixa Postal 66318, CEP 05315-970 São Paulo, SP, Brazil
[2]Department of Physics, Gomal University, Dera Ismail Khan 29220, KP, Pakistan
[3]Institute of Semiconductor Physics and Novosibirsk State University, Novosibirsk 630090, Russia
*Corresponding author. E-mail: saeedullah.phy@gmail.com

MS received 28 November 2017; revised 3 February 2018; accepted 7 February 2018;
published online 24 July 2018

Abstract. Time-resolved Kerr rotation and resonant spin amplification techniques were used to study the spin dynamics in multilayer GaAs/AlGaAs quantum wells. The spin dynamics was regulated through the wave function engineering and quantum confinement in multilayer quantum wells. We observed the spin coherence with remarkably long dephasing time $T_2^*>13$ ns for the structure doped beyond metal–insulator transition. Dyakonov–Perel spin relaxation mechanism, as well as the inhomogeneity of electron g-factor, was suggested as the major limiting factor for the spin coherence time. In the metallic regime, we found that the electron–electron collisions become dominant over microscopic scattering on the electron spin relaxation with the Dyakonov–Perel mechanism. Furthermore, the data analysis indicated that in our structure, due to the spin relaxation anisotropy, the Dyakonov–Perel spin relaxation mechanism is efficient for the spins oriented in-plane and suppressed along the quantum well growth direction resulting in the enhancement of T_2^*. Our findings, namely, long-lived spin coherence persisting up to high temperature, spin polarisation decay time with and without magnetic field, the spin–orbit field, single electron relaxation time, transport scattering time and the electron–electron Coulomb scattering time highlight the attractiveness of n-doped multilayer systems for spin devices.

Keywords. Spin coherence; quantum wells; g-factor; spin dephasing; Kerr rotation; spin–orbit field.

PACS Nos **78.20.Ls; 85.70.Sq; 75.25.−j; 76.60.Es**

1. Introduction

In recent years, the spin dynamics in semiconductor nanostructures has become the focus of intense research due to the possibility of using the spin degree of freedom in future technology [1]. Among the key requirements for successful implementation of novel spintronic devices, quantum computation and quantum information processing [2–4], a suitable system exhibiting a low relaxation rate and a long transport length [5–7] is highly desirable. Those applications could benefit from such systems because they can store and process the information before the decoherence effect sets in.

However, due to the strong coupling to its environment in a solid-state system, the spins in low-dimensional structures such as quantum wells (QWs) and quantum dots (QDs) meet a vital problem of strong dephasing. In this respect, various material structures [8–14] have been tested to control this fast decoherence. Among those materials, GaAs-based heterostructures have drawn considerable attention because of their numerous properties that make them well suited for applications in telecommunication, high frequency and high-speed electronics [15].

Recent advances in molecular beam epitaxy (MBE) enabled the engineering of new and advanced multilayer structures. By tailoring the sample geometry, thereby producing the environment to confine the carrier's wave function that penetrates into the barriers, one can witness an internal magnetic field (spin–orbit field). Such a field is believed to be the tuning force for the spin manipulation [3]. Today, most of the schemes proposed for the generation, manipulation and detection of spins rely on this internal magnetic field [16–18]. Recently, the spin–orbit effects have attracted renewed interest due to the emergence of striking phenomena such as persistent spin helix [19,20], spin Hall effect [21], large spin relaxation anisotropy [22] and Majorana fermions [23,24]. Additionally, such wave vector (**k**) driven fields induced by bulk inversion asymmetry (Dresselhaus field) [25] or structure inversion

Table 1. Studied structures where n_s and μ are the total electron density and mobility in the QW, determined by electrical transport measurements at low temperature, respectively.

Name	Structure	QW width (nm)	n_s (cm^{-2})	μ (cm^2/V s)
Sample A	DQW	45	9.2×10^{11}	1.9×10^6
Sample B	TQW	10–22–10	9.0×10^{11}	5.0×10^5
Sample C	TQW	12–26–12	9.6×10^{11}	5.5×10^5

asymmetry (Rashba field) [26] can also inherently result in spin relaxation through the Dyakonov–Perel (DP) mechanism [27].

The expectations for device applications of spin-polarised electrons will become more realistic by understanding the microscopic mechanisms responsible for the spin relaxation as well as its manifestation under different experimental conditions, e.g. applied magnetic field, sample temperature, etc. It is believed that such relaxation processes are substantially modified in the two-dimensional systems compared to the bulk [2]. While there is a vast literature on the spin relaxation process of electrons in semiconductor QWs, there are only a few investigations of carrier spin relaxation in multilayer structures. The aim of the present work was to investigate the electron spin dynamics in multilayer GaAs/AlGaAs structures. Such structures, in principle, allow the long-lived spin polarisation as well as the manipulation of those spins through the spin–orbit field [5–7,22]. Recently, the authors demonstrated that such multilayer QWs could transport coherently precessing electron spins over about half millimetres at liquid He temperature [6]. We observed the long-lived spin coherence persisting up to about room temperature. Additionally, we found a large spin relaxation anisotropy for the spins oriented in and out of plane.

The paper is organised as follows. Section 2 presents the material and experimental details. Section 3 is devoted to experimental results of spin dynamics reported in three different samples. Concluding remarks are discussed in section 4.

2. Materials and experiments

To explore the spin dynamics, we investigated here three different samples (namely A, B and C) grown by MBE on a (0 0 1)-oriented GaAs substrate. All samples are symmetrically δ-doped beyond the metal–insulator transition, where the DP spin relaxation has been reported to be more efficient [28–30]. For all the samples, the density of Si-doping was 2.2×10^{12} cm^{-2} separated from the QW by seven periods of short-period AlAs/GaAs superlattices with four AlAs and eight GaAs monolayers per period. Sample A is a 45 nm wide GaAs QW. Owing to a large well width and high electron density, the electronic system results in a double quantum well (DQW) configuration by forming a soft barrier inside the well due to the Coulomb repulsion of electrons. Sample B studied here is a triple quantum well (TQW) with a 22-nm-thick central well separated from the side wells by 2-nm-thick $Al_{0.3}Ga_{0.7}As$ barriers. Both side wells have an equal width of 10 nm. Sample C is a wide TQW having the same structure of sample B with a barrier thickness about 1.4 times thinner than that of sample B. It contains a 26-nm-thick central well and two 12-nm-thick lateral wells. For both the TQW samples, the central well width is kept wider than the lateral wells to be populated because, due to the electron repulsion and confinement, the electron density tends to concentrate mostly in the side wells. The estimated density in the side wells is 35% larger than that in the central well. The characteristics of the studied samples are summarised in table 1.

We employed the pump–probe time-resolved Kerr rotation (TRKR) [31] and resonant spin amplification (RSA) [32] techniques to monitor the spin precession of two-dimensional electron gas (2DEGs) confined in multilayer structures. A Ti:sapphire laser with 100 fs pulses and repetition frequency (f_{rep}) of 50 kHz was used for optical excitation. The laser beam was split into the pump and probe by using a beam splitter. Spin polarisation along the structure growth direction was generated by focussing the circularly polarised pump pulses at nearly normal incidence to approximately 50 μm on the sample surface. The evolution of those optically generated spin ensemble can be monitored via rotation of the polarisation plane of a linearly polarised probe pulse reflected by the sample. It is accomplished with the help of a mechanical delay line that varies the optical path length of one beam relative to the other. An external magnetic field B_{ext} is applied perpendicular to the structure growth direction (Voigt geometry) as shown in figure 1a. The external magnetic field forces the spin precesses around it. The amount of polarisation

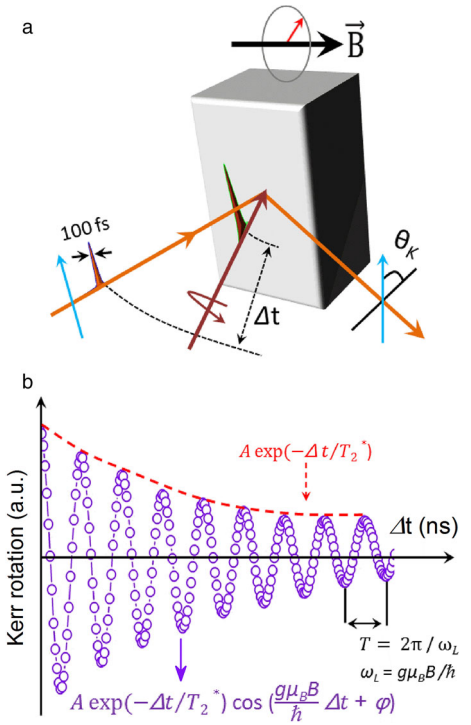

Figure 1. (**a**) Schematic of time-resolved pump–probe technique. The spin polarisation is generated by the circularly polarised pump and detected by a time-delayed weak linearly polarised probe pulse and (**b**) typical Kerr rotation (KR) signal as a function of time delay between the pump and the probe pulses.

rotation (Θ_K) of the probe beam upon the reflection on the sample is a direct measure of the amount of spin orientation at that moment. This small rotation of the direction of linear polarisation can be detected using a photodetector. A typical oscillatory response of such a TRKR experiment in the presence of an applied external magnetic field is shown in figure 1b. The frequency of oscillations is a direct measure of electron g-factor, $g = \hbar\omega_L/\mu_B B_{\text{ext}}$, while the exponential decay envelope gives a spin dephasing time T_2^*. The combination of both, spin dephasing and spin precession, leads to an exponentially decaying cosine function of the KR described by

$$\Theta_K = A\exp\left(\frac{-\Delta t}{T_2^*}\right)\cos\left(\frac{|g|\mu_B B_{\text{ext}}}{\hbar}\Delta t + \varphi\right), \qquad (1)$$

where A is the initial amplitude, μ_B is the Bohr magneton, B_{ext} is the external magnetic field, $\hbar$ is the reduced Planck constant, $|g|$ is the electron g-factor, φ is the initial phase and T_2^* is the ensemble dephasing time. The cosine factor reflects the spin precession of the external magnetic field.

3. Results and discussion

3.1 *Spin dynamics in sample A*

Figure 2a depicts the calculated DQW band structure and charge density of the two closely spaced populated subbands with separation energy $\Delta_{12} = 1.4$ meV and equal subband density n_s [33]. To find the maximum Kerr signal with long dephasing time, the TRKR measurement was carried out for different pump–probe wavelengths. The time evolution of the Kerr signal for the DQW as a function of excitation wavelengths is shown in figure 2b. For clarity of presentation, the TRKR traces are vertically shifted and normalised to $\Delta t = 0$. At higher wavelengths, the decay of spin beat is very slow, and the electron spin polarisation does not completely decay during the pulse repetition period ($t_{\text{rep}} = 13.2$ ns), and as a result one can find strong negative delay oscillation. Owing to the maximum signal at $\lambda = 817$ nm, the influence of the spin dynamics on the external magnetic field was studied keeping this wavelength for the following discussion. Figure 2c shows the pump–probe delay scan of the KR signal recorded at $T = 5$ K for various magnetic fields with a pump/probe power of 1 mW/300 μW. In the presence of an applied magnetic field, the TRKR signal results in weak damping oscillations.

To get T_2^* and electron g-factor, the TRKR traces were fitted (red curves) to eq. (1). The fitted values of ω_L (half-filled diamonds) and T_2^* (open circles) are shown in figures 2d and 2e, as a function of B_{ext}. The precession frequency increases with the magnetic field, where the linear interpolation of the data, shown by a solid red line, yields $|g| = 0.452 \pm 0.003$, which is close to the reported value of $|g| = 0.44$ for the bulk GaAs [34] and similar to the one reported for a quasi-two-dimensional system with two occupied subbands [35]. T_2^* decreases with the growing magnetic field due to the inhomogeneous spread of ensemble g-factor [10] and the DP spin relaxation mechanism [27,36]. The observed T_2^*, being limited by variation in the electron g-factor Δg, follows $1/B$-like behaviour. Data analysis allows us to estimate the size of this dispersion in g-factor by fitting the data to $1/T_2^*(B) = \Delta g\mu_B B/\sqrt{2}\hbar$ [10]. Such a fit to the data, shown by solid line, yields $\Delta g = 0.002$ which is 0.41% of the measured g-value.

The observation of spin precession at negative Δt indicates that those signals last from the previous pump pulse which overlaps with the signal from the following pulse and hence complicates the evaluation of T_2^*. In such situations, the RSA technique, based on the interference of spin polarisations generated by subsequent pulses, can be used to retrieve the accurate value of T_2^*. Figure 2f shows the KR traces obtained by scanning B_{ext}

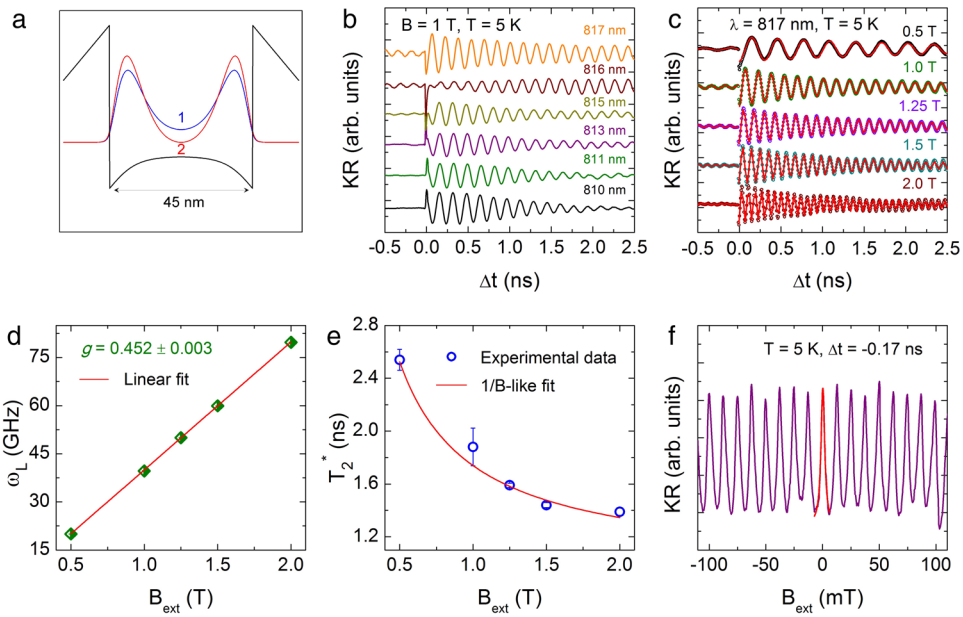

Figure 2. Spin dynamics in sample A: (**a**) DQW band structure and charge density for the two occupied subbands, (**b**) TRKR traces measured at $T = 5$ K for different excitation wavelengths, (**c**) TRKR responses measured at $\lambda = 817$ nm for different magnetic fields. Experimental traces are shown by symbols while the solid lines represent the fitted curves using eq. (1), (**d**) ω_L, (**e**) T_2^* retrieved from the fit as a function of B_{ext} and (**f**) RSA signal measured at $\Delta t = -0.17$ ns. The experimental parameters are given inside the corresponding panels.

in the range from -100 mT to $+100$ mT, while keeping Δt fixed at -0.17 ns. We observed a series of Lorentzian resonance peaks with spacing $\Delta B = hf_{\text{rep}}/g\mu_{\text{B}} \sim 12.5$ mT. The linewidth of those resonance peaks allows us to evaluate T_2^* by using a Lorentzian model [32]

$$\Theta_\kappa = A/[(\omega_L T_2^*)^2 + 1], \tag{2}$$

where $T_2^* = \hbar/g\mu_{\text{B}}B_{1/2}$ with half-width $B_{1/2}$. The fitting yields $T_2^* = 6.44 \pm 0.19$ ns which is among the longest T_2^* observed for structures with similar doping levels [30,37]. Based on the previous literature [38–40], the observed RSA signal corresponds to the regime of isotropic spin relaxation where all the peaks have the same height, and spin components of carriers oriented along the growth axis and normal to it relax at the same rate. In the opposite case, in anisotropic spin relaxation, the spin components of carriers relax at a different rate. As a result, one can see its influences on the relative amplitudes of RSA peaks.

3.2 *Spin dynamics in sample B*

The calculated band structure and charge density of the symmetric TQW (sample B) are shown in figure 3a. The thin barriers separating the wells lead to the strong tunnelling of electron states into different wells. As a result, there are three populated subbands ($i, j = 1, 2, 3$) with corresponding energy gaps $\Delta_{12} = 1.0$ meV, $\Delta_{23} = 2.4$ meV and $\Delta_{13} = 3.4$ meV, obtained from the self-consistent Hartree–Fock calculation, which are in complete agreement with the periodicity of the magneto-intersubband oscillations [41,42]. These energy gaps characterise the coupling strength between the wells. To select the right excitation energy for this sample, we first measured the KR signal vs. Δt for different pump–probe wavelengths (see figure 3b). From the experimental traces, it is clearly evident that at lower wavelengths up to 818 nm the signal displays a rapidly damping initial part transforming into a slowly decaying oscillatory tail. However, at a higher wavelength, the signal lasts longer than t_{rep} demonstrating that in this structure the signal has a maximum intensity when the excitation energy is tuned to a higher wavelength.

Figure 3c shows the TRKR traces measured at $\lambda = 821$ nm for various magnetic fields in the range from 0.4 to 2 T. According to the previous literature, in highly doped QWs, the hole contribution to the electron spin dynamics can be found as a shift of the centre of gravity of the electron spin precession [10,11,43]. In our structure, we found such a contribution at $B_{\text{ext}} = 2$ T as marked by the arrow in figure 3c. The magnetic field dependencies of ω_L and T_2^* are shown in figure 3d. The observed linear dependence of ω_L on the magnetic field gives a g-value of $|g| = 0.453 \pm 0.002$. From the B_{ext} dependence of T_2^*, one can witness a strong reduction in T_2^* with a growing field,

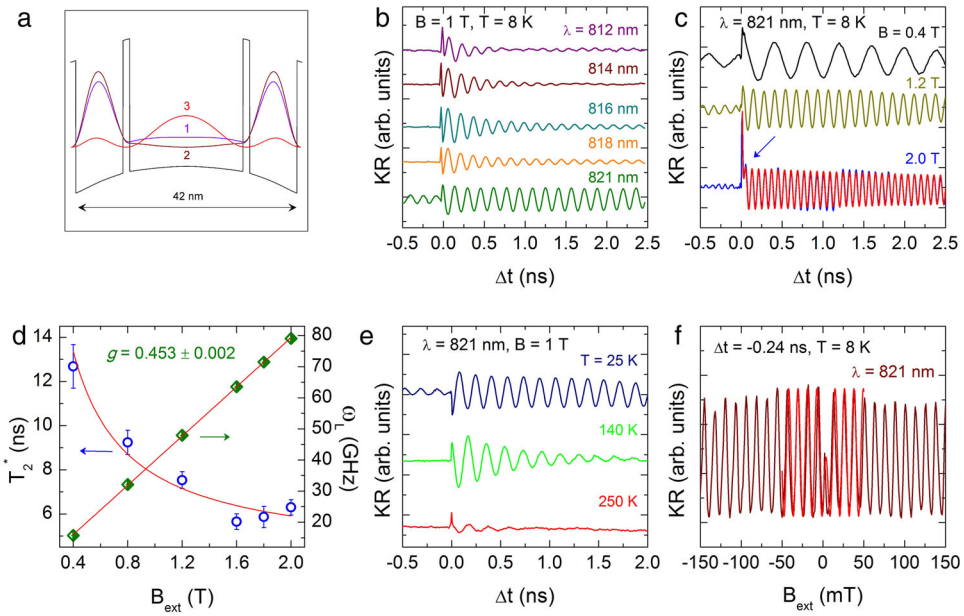

Figure 3. Spin dynamics in sample B: (**a**) TQW (sample B) band structure and charge density for the three occupied subbands with subband separation $\Delta_{12} = 1.0$ meV, $\Delta_{23} = 2.4$ meV and $\Delta_{13} = 3.4$ meV, (**b**) KR signal measured for different excitation wavelengths at $T = 8$ K, (**c**) KR as a function of Δt recorded for different magnetic fields at $\lambda = 821$ nm. The red curve on the top of experimental trace (blue) is a bi-exponential decaying cosine fit to the data. (**d**) T_2^* and ω_L as a function of an applied magnetic field, (**e**) TRKR traces recorded at various temperatures in the range up to 250 K and (**f**) RSA scan measured for $\lambda = 821$ nm.

leading to a $1/B$-like dependence. The observed dependence assumes $\Delta g = 0.0005$ (0.10% of obtained g-value). To see the influence of the sample temperature on the electron spin dynamics, the delay scan of the KR signal was carried out at three different temperatures (see figure 3e). Obviously, the signal lasts longer at low temperature as reflected by strong negative delay oscillations. Additionally, the signal is robust against temperature and was traced up to 250 K.

To avoid the contribution of variation in the ensemble g-factor to the spin relaxation process, the spin dynamics presented in figure 3f was measured in the limit of lowest possible magnetic fields. For that we used the RSA technique by scanning B_{ext} over a range of -150 to 150 mT, while keeping the delay time fixed at $\Delta t = -0.24$ ns. Fitting the zero-field RSA maximum and using the Lorentzian model lead to the out-of-plane dephasing time of 13.6 ± 2.07 ns. Apart from the long-lived spin coherence, we observed a strong spin relaxation anisotropy between the electron spins oriented in-plane and out-of-plane as is apparent from the suppression of zeroth-field peak compared to the side peaks. The observed anisotropy has its origin in the presence of an internal magnetic field. The magnitude and direction of this internal field can be inferred by fitting the data to the model described in [22,44]. Such a fitting, displayed in a selected range (from -50 to 50 mT) for clarity, yields an internal field magnitude of $B_\perp = 3$ mT. A detailed study of spin relaxation anisotropy as a function of experimental parameters (namely, sample temperature, pump–probe delay and optical power) can be found in [22]. The observed long T_2^* in the out-of-plane direction for both samples A and B stipulates that the scattering-induced DP mechanism is weak in the studied structures [12]. However, combined with the inhomogeneous spread of g-factor, it leads to a strong T_2^* reduction.

3.3 *Spin dynamics in sample C*

Finally, we report on the spin dynamics of sample C. The band structure and charge density of this structure with the three populated subbands are shown in figure 4a. Contrary to the DQW, we noted that for both the TQWs the third subband has the opposite charge distribution compared to the first and second subbands. The third subband has charge density localised in the central well, while the electrons in the lower subbands are more distributed in the side wells. The TRKR signals measured by the changing excitation wavelength of the laser pulses over the range from 811 to 821 nm, while keeping the same pump power under an external magnetic field of 1 T, are shown in figure 4b. From the experimental curves, it is clearly evident that the decay of the KR signals is changing with excitation wavelengths that are only for lower wavelengths, the spin precession

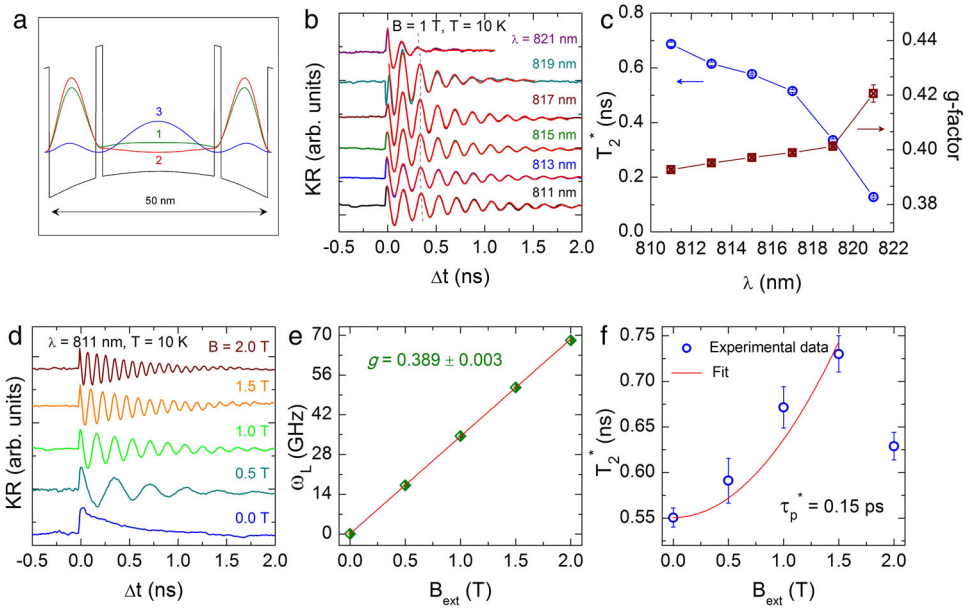

Figure 4. Spin dynamics in sample C: (**a**) sample C band structure and charge density for the three occupied subbands, (**b**) TRKR traces recorded at $T = 10$ K for different pump–probe wavelengths (coloured) and fits to the data (red). The spin beats live longer at lower wavelengths. (**c**) The relative T_2^* and g-factor evaluated from (b), (**d**) dependence of Kerr signal on external magnetic fields and corresponding (**e**) ω_L and (**f**) T_2^*.

lasting up to $\Delta t = 2$ ns. To obtain the information of spin dephasing time and electron g-factor, the precessional signal was fitted with a mono-exponential decaying cosine function as shown by red curves plotted on the top of experimental data. The obtained T_2^* and g-factor are shown in figure 4c. A clear variation of spin dephasing time is observed with the increase of laser detuning having the maximum at 811 nm. Additionally, the electron g-factor shows a variation of 0.028, due to the change in precession frequency as marked by the dashed line, in the measured range of wavelengths.

To investigate the dependence of spin dynamics on the applied magnetic field, a series of TRKR measurements for the wavelength with a maximum KR signal were performed at $T = 10$ K. Figure 4d shows TRKR scans measured with no magnetic field and in the transverse magnetic field up to 2 T. In the frame of the DP spin relaxation mechanism, the observed signal at $B_{\text{ext}} = 0$ corresponds to the strong scattering regime [5]. Unlikely, in the weak scattering regime, the electrons spin precess about the spin–orbit field by one or more revolutions before scattering and hence leading to an oscillatory behaviour [45]. From the TRKR signals, the dependence of spin dephasing time and Larmor frequency on the applied magnetic field is shown in figures 4e and 4f. The linear dependence of Larmor frequency on the applied magnetic field yields an effective Lande factor of 0.389 ± 0.003, which is in agreement with the magnitude of g-value reported previously on the same sample [6].

Additionally, with the growing magnetic field up to 1.5 T, we observed a monotonous increase in T_2^*. In such a situation, B_{ext} leads to the cyclotron motion of conduction band electrons which lets the direction of **k** to change, thereby suppressing the precession around the random internal magnetic field. As a result, the electron spin preserves its initial spin orientation, and thus is inconsistent with the DP mechanism [46], leading to the enhancement of T_2^*. This is the key difference compared to samples A and B, where the cyclotron effect is suppressed and the DP mechanism is more efficient. The dependence of T_2^* on the applied magnetic field follows a quadratic dependence given as [37,46]

$$T_2^*(B) = T_2^*(0)/(1 + \omega_c^2 \tau_p^2). \tag{3}$$

Here, $T_2^*(0)$ is the zero-field spin relaxation time, ω_c is the cyclotron frequency and τ_p is the single-electron relaxation time, which is defined as the inverse sum of transport scattering rate and electron–electron scattering rate [5]:

$$\tau_p = (\tau^{-1} + \tau_{ee}^{-1})^{-1}. \tag{4}$$

From the fit (solid red curve) to the data, we retrieved $\tau_p = 0.15$ ps which is in agreement with the magnitude of quantum lifetime reported by transport for a similar TQW sample [41]. The transport scattering time was estimated using the electron charge e and effective mass

m^*, by $\tau = \mu m^*/e = 20$ ps, which is quite different from τ_p. The observed large difference was associated with the fact that τ includes only the large-angle scattering, while τ_p is caused by all kinds of scattering events. The ratio of measured τ and τ_p determines the nature of the dominant scattering mechanism [47]. For GaAs-based heterostructures, it was assumed that $\tau/\tau_p \lesssim 10$ for background impurity scattering and $\tau/\tau_p \gtrsim 10$ for the remote ionised impurity scattering [47]. The observed $\tau/\tau_p \approx 135$ indicates that the dominant scattering in our structure is caused by remote instead of background impurities. The electron–electron scattering time (τ_{ee}) can be approximated by using eq. (4) which leads to $\tau_p \approx \tau_{ee}$ demonstrating the supremacy of electron–electron scattering over microscopic scattering mechanisms [48].

4. Conclusions and outlook

In summary, we have studied the electron spin dynamics in high-mobility two-dimensional electron gases using the pump–probe reflection techniques: TRKR and RSA. The DQW structure yields $T_2^* = 6.44$ ns, while in the TQW, we observed a strikingly long T_2^* exceeding the laser repetition. In the wide TQW, T_2^* increases with the applied magnetic field but is much smaller than that in the DQW and other TQW. Additionally, we observed that the anisotropic feature is most likely due to the presence of an internal magnetic field. The observed long-lived spin coherence persists up to about room temperature, with encouraging indication for spin optoelectronics and particularly the long spin memories in multilayer GaAs QWs. We believe that determination of all the relevant time scales will be useful for the future spintronics devices and quantum information processing.

Acknowledgements

FGGH acknowledges the financial support from Grant Nos 2009/15007-5, 2013/03450-7, 2014/25981-7 and 2015/16191-5 of the São Paulo Research Foundation (FAPESP). SU acknowledges TWAS/CNPq for the financial support.

References

[1] S A Wolf, *Science* **294**, 1488 (2001)
[2] M I Dyakonov, *Spin physics in semiconductors* (Springer-Verlag, Berlin, 2008)
[3] D D Awschalom, D Loss and N Samarth, *Semiconductor spintronics and quantum computation* (Springer-Verlag, Berlin, 2002)
[4] F Henneberger and O Benson, *Semiconductor quantum bits* (Pan Stanford, Singapore, 2009)
[5] S Ullah, G M Gusev, A K Bakarov and F G G Hernandez, *J. Appl. Phys.* **119**, 215701 (2016)
[6] F G G Hernandez, S Ullah, G J Ferreira, N M Kawahala, G M Gusev and A K Bakarov, *Phys. Rev. B* **94**, 045305 (2016)
[7] S Ullah, G J Ferreira, G M Gusev, A K Bakarov and F G G Hernandez, *J. Phys.: Conf. Ser.* **864**, 012060 (2017)
[8] R Bratschitsch, Z Chen, S T Cundiff, E A Zhukov, D R Yakovlev, M Bayer, G Karczewski, T Wojtowicz and J Kossut, *Appl. Phys. Lett.* **89**, 221113 (2006)
[9] J Lohrenz, T Paschen and M Betz, *Phys. Rev. B* **89**, 121201(R) (2014)
[10] E A Zhukov, D R Yakovlev, M Bayer, G Karezewski and T Wojtowiez, *Phys. Status Solidi B* **243**, 878 (2006)
[11] E A Zhukov, D R Yakovlev, A Schwan, O A Yugov, A Waag, L W Molenkamp and M Bayer, *Phys. Status Solidi B* **251**, 1872 (2014)
[12] J Lee, A Venugopal and V Sih, *Appl. Phys. Lett.* **106**, 012403 (2015)
[13] S Ghosh, V Sih, W H Lau, D D Awschalom, S-Y Bae, S Wang, S Vaidya and G Chapline, *Appl. Phys. Lett.* **86**, 232507 (2005)
[14] H Mino, Y Kouno, K Oto, K Muro, R Akimoto and S Takeyama, *Appl. Phys. Lett.* **92**, 153101 (2008)
[15] A Baca and C Ashby, *Fabrication of GaAs devices* (Institution of Engineering and Technology, UK, 2005)
[16] S Datta and B Das, *Appl. Phys. Lett.* **56**, 665 (1990)
[17] T Koga, J Nitta, H Takayanagi and S Datta, *Phys. Rev. Lett.* **88**, 126601 (2002)
[18] H Cruz and D Luis, *J. Appl. Phys.* **104**, 083715 (2008)
[19] J D Koralek, C P Weber, J Orenstein, B A Bernevig, S-C Zhang, S Mack and D D Awschalom, *Nature* **458**, 610 (2009)
[20] M P Walser, C Reichl, W Wegscheider and G Salis, *Nat. Phys.* **8**, 757 (2012)
[21] F G G Hernandez, L M Nunes, G M Gusev and A K Bakarov, *Phys. Rev. B* **88**, 161305(R) (2013)
[22] S Ullah, G M Gusev, A K Bakarov and F G G Hernandez, *J. Appl. Phys.* **121**, 205703 (2017)
[23] R M Lutchyn, J D Sau and S D Sarma, *Phys. Rev. Lett.* **105**, 077001 (2010)
[24] Y Oreg, G Refael and F V Oppen, *Nat. Phys.* **105**, 177002 (2010)
[25] G Dresselhaus, *Phys. Rev.* **100**, 580 (1955)
[26] Y A Bychkov and E L Rashba, *J. Phys. C* **17**, 6039 (1984)
[27] M I Dyakonov and V I Perel, *Sov. Phys.–JETP* **33**, 1053 (1971)
[28] R I Dzhioev, K V Kavokin, V L Korenev, M V Lazarev, B Y Meltser, M N Stepanova, B P Zakharchenya, D Gammon and D S Katzer, *Phys. Rev. B* **66**, 245204 (2002)
[29] M Römer, H Bernien, G Müller, D Schuh, J Hübner and M Oestreich, *Phys. Rev. B* **81**, 075216 (2010)

[30] J S Sandhu, A P Heberle, J J Baumberg and J R A Cleaver, *Phys. Rev. Lett.* **86**, 2150 (2001)
[31] J J Baumberg, D D Awschalom, N Samarth, H Luo and J K Furdyna, *Phys. Rev. Lett.* **72**, 717 (1994)
[32] J M Kikkawa and D D Awschalom, *J. Phys. C* **80**, 4313 (1998)
[33] S Wiedmann, G M Gusev, O E Raichev, A K Bakarov and J C Portal, *Phys. Rev. B* **84**, 165303 (2011)
[34] O Madelung, *Semiconductors: Basic data*, 2nd edn (Springer, Berlin, 1996)
[35] F Zhang, H Z Zheng, Y Ji, J Liu and G R Li, *Europhys. Lett.* **83**, 47007 (2008)
[36] M I Dyakonov and V I Perel, *Sov. Phys.–Semicond.* **20**, 110 (1986)
[37] A V Larionov and A S Zhuravlev, *JETP Lett.* **97**, 137 (2013)
[38] M M Glazov and E L Ivchenko, *Semiconductors* **42**, 951 (2008)
[39] I A Yugova, M M Glazov, D R Yakovlev, A A Sokolova and M Bayer, *Phys. Rev. B* **85**, 125304 (2012)
[40] M Griesbeck, M M Glazov, E Y Sherman, D Schuh, W Wegscheider, C Schüller and T Korn, *Phys. Rev. B* **85**, 085313 (2012)
[41] S Wiedmann, N C Mamani, G M Gusev, O E Raichev, A K Bakarov and J C Portal, *Phys. Rev. B* **80**, 245306 (2009)
[42] S Wiedmann, N C Mamani, G M Gusev, O E Raichev, A K Bakarov and J C Portal, *Physica E* **42**, 1088 (2010)
[43] D R Yakovlev and M Bayer, in: *Spin physics in semiconductors* edited by M I Dyakonov (Springer, Berlin, 2008)
[44] B M Norman, C J Trowbridge, D D Awschalom and V Sih, *Phys. Rev. Lett.* **112**, 056601 (2014)
[45] M Griesbeck, M M Glazov, T Korn, E Y Sherman, D Waller, C Reichl, D Schuh, W Wegscheider and C Schüller, *Phys. Rev. B* **80**, 241314 (2009)
[46] G Wang, A Balocchi, A V Poshakinskiy, C R Zhu, S A Tarasenko, T Amand, B L Liu and X Marie, *New J. Phys.* **16**, 045008 (2014)
[47] S J MacLeod, K Chan, T P Martin, A R Hamilton, A See, A P Micolich, M Aagesen and P E Lindelof, *Phys. Rev. B* **80**, 035310 (2009)
[48] W J H Leyland, G H John, R T Harley, M M Glazov, E L Ivchenko, D A Ritchie, I Farrer, A J Shields and M Henini, *Phys. Rev. B* **75**, 165309 (2007)